Cyano-Functionalized Triarylamines on Au(111)

Gottardi, Stefano; Müller, Kathrin; Moreno Lopez, Juan Carlos; Yildirim, Handan; Meinhardt, Ute; Kivala, Milan; Kara, Abdelkader; Stöhr, Meike

Published in:
Advanced Materials Interfaces

DOI:
10.1002/admi.201300025

Publication date:
2014

Article type: Full Paper

Title: Cyano-Functionalized Triarylamines on Au(111): Competing Intermolecular vs. Molecule/Substrate Interactions

Stefano Gottardi[+], Kathrin Müller[+], Juan Carlos Moreno-López, Handan Yildirim, Ute Meinhardt, Milan Kivala*, Abdelkader Kara, Meike Stöhr**

([+]contributed equally)

S. Gottardi, Dr. K. Müller, Dr. J. C. Moreno-López, Dr. M. Stöhr

Zernike Institute of Advanced Materials

University of Groningen

Nijenborgh 4, 9747 AG Groningen, the Netherlands

E-mail: k.muller@rug.nl

m.a.stohr@rug.nl

Dipl.-Chem. U. Meinhardt, Dr. M. Kivala

Chair of Organic Chemistry 1, Department of Chemistry and Pharmacy,

University of Erlangen-Nürnberg,

Henkestrasse 42, 91054 Erlangen, Germany

E-Mail: milan.kivala@fau.de

Dr. H. Yildirim, Prof. Dr. A. Kara

Department of Physics, University of Central Florida, Orlando,

Florida 32816, USA

Keywords: self-assembly, dipolar coupling, cyano functional group, scanning tunneling microscopy, triarylamines

Abstract

The self-assembly of cyano-substituted triarylamine derivatives on Au(111) is studied with scanning tunneling microscopy and density functional theory calculations. Two different phases, each stabilized by at least two different cyano bonding motifs are observed. In the first phase, each molecule is involved in dipolar coupling and hydrogen bonding, while in the second phase, dipolar coupling, hydrogen bonding and metal-ligand interactions are present. Interestingly, the metal-ligand bond is already observed for deposition of the molecules with the sample kept at room temperature leaving the herringbone reconstruction unaffected. We propose that for establishing this bond, the Au atoms are slightly displaced out of the surface to bind to the cyano ligands. Despite the intact herringbone reconstruction, the Au substrate is found to considerably interact with the cyano ligands affecting the conformation and adsorption geometry, as well as leading to correlation effects on the molecular orientation.

1. Introduction

Supramolecular structures on surfaces have been studied intensely over the past decades to obtain fundamental insight into the mechanisms governing molecular self-assembly. A detailed understanding of the growth is of utmost importance to successfully implement such self-assembled organic nanomaterials in devices for electronic, optoelectronic and sensor applications.[1] It is well known that the subtle interplay between intermolecular and adsorbate/surface interactions plays a crucial role in the self-assembly process.[2] The intermolecular interactions are generally of non-covalent nature including hydrogen bonding,[3] dipole-dipole interactions,[4] metal coordination[5] and van der Waals (vdW) forces.[6] The adsorbate/surface interaction is influenced by the corrugation of the adsorption potential (i.e. the variation of the adsorption energy for different adsorption positions and molecular orientations), the reactivity of the substrate, the crystal structure and potential surface reconstructions.

With the help of specific functional groups, control over the molecular self-assembly is obtained. Such ligand groups can drive the assembly towards 0D clusters,[7,8] 1D chains[9] or 2D extended networks.[10] Due to self-recognition and error correction, which are inherent for non-covalent bonding and which happen via bond formation and bond breaking until an equilibrium structure is formed, highly organized, defect-free structures can develop.

Cyano-functionalized molecules have gained increasing interests over the last years because the asymmetric charge distribution of cyano ligands leads to the formation of an intrinsic dipole, which can be involved in intermolecular dipolar coupling or hydrogen bonding.[11] Additionally, cyano groups (CN-groups) can undergo metal-ligand interactions resulting in the formation of highly stable structures.[7,12, 13] In this respect, the self-assembly of dicarbonitrile polyphenyl derivatives on Ag(111) was extensively studied.[14,15,16] For room temperature deposition and coverages below one monolayer, the observed structures are stabilized by hydrogen bonding while the co-deposition of metal atoms leads to the formation of hexagonal metal-coordinated porous networks, whose pore size can be steered by the

number of phenyl rings per molecule.[17] Another well-studied example are cyano-substituted porphyrins [4,7] for which the number and position of the cyano groups determine the adsorption geometry.

Herein, we report on the investigation of an achiral tricyano-substituted triarylamine derivative (4,4,8,8,12,12-hexamethyl-4*H*,8*H*,12*H*-benzo[1,9]quinolizino[3,4,5,6,7-*defg*]acridine-2,6,10-tricarbonitrile) denoted as **1** (cf. Figure 1a)[18] in which the sp^3-hybridized dimethylmethylene tethers lead to a virtually planar conformation of the originally propeller-shaped triarylamine moiety. These planarized triarylamines, so-called heterotriangulenes,[19] are currently experiencing a vigorous renaissance as versatile building blocks for functional optoelectronic materials.[20] In particular, various derivatives of dimethylmethylene-bridged triarylamines were shown to act as promising hole conductors with superior stability in light-emitting devices[21] or as efficient chromophores for dye-sensitized solar cells.[22]

Compound **1** used in the present study has a triangular shape with terminal CN-groups at each vertex (**Figure 1**a). As substrate we chose Au(111), which is generally less reactive in comparison to other coinage metals like Ag and Cu, since we wanted to minimize the influence of the substrate on the formation of molecular overlayers. Although, it is known that the herringbone reconstruction of Au(111) can influence the adsorption behavior, e.g. by leading to preferential adsorption on elbows, hcp or fcc sites.[23] The aim was to investigate the influence of the geometrical arrangement of the cyano functionalities – also taking into account the molecular shape – on the self-assembly process. At first glance, antiparallel dipolar coupling should be the dominant intermolecular interaction motif[11] resulting in the formation of porous networks. Instead and to our surprise, we observed two-dimensional adsorption structures, which are simultaneously stabilized by several types of interactions: either dipolar coupling and H-bonding, or dipolar coupling, metal-ligand interactions and hydrogen bonding. It should be noted that to the best of our knowledge most of the reported

molecular structures formed by cyano-functionalized building blocks are based on only one type of intermolecular interaction. However, Pawin et al.[13] and Reichert et al.[24] reported the presence of metal coordination and hydrogen bonding at the same time. These structures are due to a metal deficiency and with excess metal ad-atoms only metal coordinated bonds are present. On the other hand, Kühne et al.[15] observed structures stabilized by hydrogen bonding and dipolar coupling. Moreover, the Au substrate was found to be not as passive as supposed. By analyzing the correlation probability, the influence of the Au(111) substrate on the molecular orientation became apparent. In the following, we will present the different adsorption structures observed and discuss the delicate interplay of the various interactions. Our experimental observations are complemented by density functional theory (DFT) calculations, which give further insight into the intricate bonding scenario.

2 Results

2.1 Experimental results

Individual molecules of **1** examined with scanning tunneling microscopy (STM) exhibit a triangular shape. In high resolution STM images, these triangles show three protrusions (Figure 1c). The bright contrast results from the out of plane methyl groups[25] as indicated by the overlaid structure model of one molecule in Figure 1c. On the contrary, the CN-groups are not imaged by STM, and extend perpendicularly to the edges of the triangle. The simulated STM image agrees well with the assignment of the bright contrast to the methyl groups (Figure 1b). Based on this triangular contrast, the molecular orientation in the tentative structure models shown below for the different adsorption structures could be assigned univocally.

Figure 2a shows an STM image obtained for the Au(111) surface covered with one monolayer (ML) of **1**. At such a coverage, the formation of a hexagonal close-packed

arrangement is favored, denoted as close-packed phase α throughout the paper. The Au(111) herringbone reconstruction[26] is clearly visible through the molecular overlayer, and seems not affected by adsorption of the molecules. From a detailed analysis of the obtained STM images and low-energy electron diffraction (LEED) data (see SI), two domains of the close-packed phase α can be identified, which differ by a rotation of the unit cell vectors of ±11° with respect to the [$1\bar{1}0$]-direction of the substrate, indicated by the black arrow in Figure 2c.

The tentative adsorption structure of one domain is shown in Figure 2c. It can be described by the adsorption matrix $\begin{pmatrix} 5 & 1 \\ -1 & 4 \end{pmatrix}$, assuming a commensurate superstructure with respect to the unreconstructed Au(111) surface. The unit cell contains one molecule and its dimensions are $a = b = 1.32$ nm, and $\theta = 120°$ resulting in a molecular density of 0.66 molecules/nm^2.

The arrangement of the molecules within phase α clearly exhibits chirality (Figure 2c). This can be recognized by the position of the CN-group of one molecule with respect to the neighboring molecule: for right handed chirality one molecule always points left to the center of the neighboring molecule. For the domain exhibiting left handed chirality, the CN-groups always point to the right side of the neighboring molecules. This type of chirality, which occurs by the adsorption of achiral molecules on a surface due to the specific alignment of neighboring molecules is called organizational chirality.[27] Left and right handed homochiral domains are shown in the SI (Figure S1d).

In Figure 2b the triangular shape of the molecules is visible. Hereby, two possible molecular orientations characterized by a 60° rotation with respect to each other can be distinguished. The two different orientations become clearly visible in the tentative structure model (Figure 2c). These different molecular orientations lead to different intermolecular interactions: (i) Dipolar coupling between CN-groups of two adjacent molecules (red oval in Figure 2c) called CN-CN bond. This coupling is characterized by an antiparallel orientation of the cyano ligands of neighboring molecules. The distance between the center of the C-atom of

the CN-group and the N-atom of the neighboring molecule's CN-group is approximately 3.3 Å , which agrees well with theoretical calculations for this bonding motif.[11] Note that this bond is additionally stabilized by hydrogen bonding to the phenyl hydrogen of the neighboring molecule. (ii) Hydrogen bonding (light blue oval in Figure 2c) between the nitrogen atom of the CN-group and a hydrogen atom of the phenyl ring of a neighboring molecule, called CN-HC in the following. The N···H distance for this bond is approximately 1.8 Å, as derived from the tentative adsorption structure model. (iii) Trimeric motif (dark blue circle in Figure 2c); for this configuration all three molecules are oriented in the same direction leading to three CN-HC bonds similar to the one discussed previously. The distance between the C-atom of one CN-group and the N-atom of the neighboring CN-group is 3.5 Å, in agreement to the distances calculated by Okuno *et al.*[28].

In the following, the relationship between the two different orientations of the molecules, which are found in the close-packed phase α, will be discussed in more detail. The rectangle in Figure 2a indicates the area of the STM image, which was used to analyze the correlation between the different molecular orientations.[29] All three high symmetry directions of the close-packed phase α were considered, which are indicated by the colored arrows in Figure 2a. Figure 2d shows the result for direction 1 (79° w.r.t. herringbone reconstruction lines) and direction 2 (41° w.r.t. herringbone reconstruction lines). The result for direction 3, (19° w.r.t. herringbone reconstruction), is reported in the SI. A clear modulation in the correlation function is visible for direction 1 and 2, resembling the distance between the gold reconstruction lines along these directions: about 5 molecular units for direction 1 and about 8 molecular units for direction 2. In contrast, direction 3 does not show a periodicity in the correlation because it is nearly parallel to the herringbone reconstruction. The noise for direction 2 and 3 is higher due to less statistics along these directions because of the change in the orientation of the herringbone reconstruction lines (see Figure 2a). The modulation in the correlation function with a periodicity resembling the distance of the

herringbone reconstruction lines along the molecular rows is a clear indication that the substrate has an influence on the orientation of the molecules in the close-packed phase α. We believe that this correlation is the result of a competition between intermolecular interactions – the molecules tend to form the strongest possible bonds – and molecule/substrate interaction.

Figure 3 shows an overview STM image obtained after submonolayer deposition of **1**. Here, besides the free metal, two different molecular phases are present: phase *α* and a new phase that will be named phase *β* in the following. The latter is visible in the top part of Figure 3 and will be described in detail later.

For submonolayer coverage, phase *α* shows the presence of numerous vacancies, which can result in the formation of a porous network (**Figure 4**). The unit cell of the porous phase *α* is rotated by 30° with respect to the unit cell of the close-packed phase *α*, i.e. a rotation of ±41° with respect to the [$1\bar{1}0$] direction of Au(111). The adsorption structure can be described by a $\begin{pmatrix} 9 & 0 \\ -6 & 3 \end{pmatrix}$ matrix with respect to the unreconstructed Au(111) surface, with two molecules per unit cell (see Figure 4c for a tentative adsorption structure model). The unit cell vectors measure $a = b = 2.29$ nm, $\theta = 120°$ and the density is 0.44 molecules/nm^2, in contrast to 0.66 molecules/nm^2 for the close-packed phase *α*.

The molecules forming one pore arrange in such a way that neighboring molecules are rotated by 60° with respect to each other. Thus, each pore is formed by six molecules arranged in a circular motif. The molecules interact exclusively via dipolar antiparallel coupling as it is the case in the bonding motif shown by the red oval in Figure 2c; this can be seen in the structure model displayed in Figure 4c. Also the porous phase *α* exhibits chirality, which is expected as this phase derives from the chiral close-packed phase *α*.

Figure 5 shows the second phase, which was observed for submonolayer coverage: phase *β*. The Au(111) herringbone reconstruction remains intact underneath the molecular network and seems not affected by the molecular ad-layer (Figure S4 in SI). Also this phase shows areas with pores as well as filled areas similar to phase *α*. The pores consist of six molecules aligned in the same circular motif as the one observed for the porous phase *α*.

A detailed analysis of the obtained STM data and comparison with phase *α* shows that the unit cell of phase *β* is rotated by ± 23° with respect to the Au [$1\bar{1}0$] direction with the unit cell vectors measuring $a = b = 3.77$ nm and $\theta = 120°$. The unit cell contains six molecules in the case of the porous structure, which is shown in Figure 5c and can be described by a $\begin{pmatrix} 15 & 6 \\ -6 & 9 \end{pmatrix}$ matrix with respect to unreconstructed Au(111), assuming a commensurate superstructure. The filled phase *β* has a density of 0.49 molecules/nm^2 and the porous phase *β* has a density of 0.42 molecules/nm^2.

The main difference between phase *α* and phase *β* is the connection of neighboring pores. While for the porous phase *α* two neighboring pores share two molecules, the neighboring pores in phase *β* do not share any molecules, i.e. they are isolated from each other. For phase *β*, three adjacent pores are connected via a threefold unit where each pore contributes with one molecule. Within this threefold unit the partially negatively charged N-atoms of the polar CN-groups point directly towards each other (blue circle in Figure 5c). This configuration is energetically unfavorable due to the electrostatic repulsion between the N-atoms. At the first glance, the trimeric motif observed for phase *α* would be expected. Such a trimeric unit can be achieved by rotating each entire circular unit, containing six molecules, by 6°. However, this can be excluded due to the following reasons: (i) The CH···N distance for establishing hydrogen bonding between adjacent molecules (Figure S5) is much larger (3.7 Å) than for hydrogen bonds reported in literature (2.7 - 2.9 Å).[28,30] (ii) This structure model does not fit with the STM images when superimposed (see Figure S6 in SI). For these

reasons we propose that this threefold unit is stabilized by metal-ligand bonding with the CN-groups. The coordination of CN-groups to transition metal atoms is well-known from supramolecular chemistry[31] and was reported for two-dimensional surface supported networks.[7,17,32] Moreover, 2D Au metal coordinated molecular networks were recently fabricated.[12,33] The distance of 2 Å measured between the center of the N-atoms of the CN-groups and the center of the threefold unit agrees well with values reported for metal ligand interactions.[12] Further support for the proposed metal-ligand bond is found by looking at the edges of phase β islands (Figure 3 and Figure S7): They are terminated by threefold units indicating that these units can only exist as a whole. Furthermore, the STM signal reveals brighter contrast at the center of the threefold units for high positive tunneling biases (>2.0 V) (Figure 5b). Such an enhanced contrast was also observed for other metal-coordinated structures,[34] but was not observed in-between the molecules in phase α and hence, is another indication for the metal-ligand bond (cf. SI Figure S8).

Two different bonding motives – metal-ligand bonding (interaction between neighboring pores) and dipolar coupling (interaction within the pores) stabilize the porous phase β. For the filled phase β, a third bonding motif is present. The additional molecule in the pore interacts with three of the six molecules forming the pore via hydrogen bonding (see light blue oval in Figure 2c).

Also phase β is chiral, because the antiparallel dipolar coupling between neighboring molecules in the circular motifs leads to organizational chirality.[27] Thereby, homo-chiral domains, one with left-handed chirality and the other with right-handed chirality, were observed for phase α and β (see **Figure 6**).

2.2 Theoretical results

DFT calculations of the molecules in the gas phase were performed using different functionals (PBE, optB86b and optB88) to further investigate the relative stability of the different bonding motifs observed for the close-packed phase *α*. For this analysis, two or three molecules were brought close together (about 3 Å distance) to form the desired motif, and then the system was allowed to relax. The studied motifs were antiparallel dipolar coupling between CN-groups (shown by the red oval in Figure 2c), hydrogen bonding (shown by the light blue oval in Figure 2c), and the trimeric motif (shown by the dark blue oval in Figure 2c). The DFT-optimized structures of the bonding motifs are shown in **Figure 7** along with the obtained intramolecular distances within one molecule (Figure 7a top). These intramolecular bonding distances are similar to those of the single molecule, and do not change when the molecules are brought close together.

In **Table 1**, the results obtained for the binding energy as well as the intermolecular bond lengths (see colored arrows in Figure 7), which are relevant for each of the bonding motifs, are summarized. Independent of the functional used, we find that the CN-CN bond is the energetically most favorable configuration with a N···C distance of approximately 3.5 Å (see blue arrow in Figure 7a), which is similar to the earlier reported results for dipolar coupling of CN-groups.[11,28] The CN-groups are almost parallel to each other (see Figure 7a). The trimeric motif is the second most stable configuration with a slightly lower binding energy per molecule-molecule bond (Figure 7c). The CN-HC motif is the least stable motif out of the three studied ones (see Figure 7b) with a N···H distance of approx. 2.2 Å (shown by the red arrow in Figure 7b). This distance is slightly smaller than the one calculated for a benzonitrile dimer (approx. 2.7Å)[28] and also smaller than the one reported for the Proton Acceptor Ring Interaction (PARI) (2.9 Å).[30] However, for the configuration reported here the N-atom points directly to the only available H-atom of the phenyl ring, while for PARI the N-atom points in between two neighboring H-atoms of the phenyl ring.

Additional to the gas phase calculations, the adsorption of a single molecule on the non-reconstructed Au(111) surface was studied using the same functionals as for the gas phase calculations. The main interest is to determine the adsorption geometry of the molecule. Our calculations show that the adsorption energies depend strongly on the functional used. While the adsorption energy obtained using PBE is only 80 meV suggesting weak adsorption, those calculated using the optB86b and optB88 are 2.86 eV and 2.89 eV, respectively. The values obtained with the vdW functionals indicate a high adsorption strength, while the standard PBE cannot capture the accurate binding nature.[35,36,37] Despite the high adsorption energy obtained using optB86b and optB88 functionals, the energy landscape is very shallow, i.e. the binding energy between the molecule and the Au(111) surface changes only slightly for different adsorption positions.

Our results obtained using optB86b and optB88 functionals indicate that the molecule, adsorbed on the Au(111) surface, undergoes arching in contrast to the gas phase, for which the structural analysis suggests that the backbone of the molecule is flat (see Figure 7) regardless of the functional used. However, upon adsorption, the results obtained using the optB86b functional show that the CN-groups arch towards the surface with the N···Au distance becoming 2.7 Å, while the central N-atom is 4 Å away from the Au(111) surface. The bending of the CN-groups towards the metal surface is consistent with earlier reports[28,38,39] and can be explained by the formation of a mirror image charge in the Au substrate induced by the dipole of the CN-group.[28] The distance between the C-atoms of the CN-group and the Au(111) surface is 3 Å. In contrast, the bridging dimethyl groups are rotated away from the surface upon adsorption resulting in 3.7 Å distance between the C-atom of the lower methyl group and the Au(111) surface. Consequently, all methyl groups are visible in the top view as shown in **Figure 8a**. The results obtained using the optB88 functional show very similar binding energy values and adsorption configuration, while the PBE results show almost no arching upon adsorption of the molecule. The top layer atoms of

the substrate show no buckling when we performed the calculations using PBE, while buckling of 0.08 Å is encountered when the optB86b and opt B88 functionals are used.

In Figure 8b and c, the side views of the adsorption geometry of the molecule on Au(111) together with the charge density difference calculated using the optB86b functional is shown, viewed either from the CN- or methyl-groups. Here, the details of the adsorption geometry of the molecule can be identified and both arching of the whole molecule and rotation of the methyl groups becomes clearly visible. The charge density difference shown in Figure 8 is calculated by subtracting the charge densities of the molecule and the substrate alone from that of the molecule adsorbed on the Au(111) surface. The blue and red colors represent the regions with depletion and accumulation of charge, respectively. The charge density difference plots show that charge accumulation occurs in the CN-groups, which is due to close proximity of the N-atoms to the surface atoms. A slight change in the charge distribution is also visible in the Au-atoms underneath the CN-groups. In contrast, almost no change in the charge density of the central N atom was observed.

3. Discussion

Previously, it has been reported that for large π-conjugated molecules a simple discrimination of physisorption vs. chemisorption based on the binding energy alone is not possible.[35,40] The fact that the herringbone reconstruction of the Au(111) surface remains intact underneath the adsorbed molecules is generally considered as a sign for a weak molecule/substrate interaction[41] suggesting a physisorption-type interaction. However, in our case the following observations contradict a weak molecule/substrate interaction: (i) The step edges show a rearrangement when the molecules grow over them (Figure S3b in the SI). (ii) The correlation of the molecular orientation in the close-packed phase α with respect to the herringbone reconstruction indicates a considerable influence of the substrate on the

molecular arrangement. (iii) DFT calculations with the inclusion of vdW interactions show a large adsorption energy of 2.9 eV as well as arching of the molecule when adsorbed on the Au(111) surface. Additionally, an electronic redistribution occurs upon adsorption of the molecule on the gold surface, as seen by the charge density difference plots in Figure 8b and c. This strong molecule/substrate interaction is mediated by the cyano/gold interaction.

DFT calculations show a relatively shallow landscape of the binding energy for different adsorption sites on the Au(111) surface. Additionally, the geometrical structure of the molecules changes when they adsorb on the surface, as seen by the arching of the molecule and upward rotation of the methyl groups. This flexibility in both, the adsorption position and in the conformation of the molecules, can be used in the self-assembly to form an adsorption structure which is in a lower energetic minimum. In this way, the molecules can also adjust to the corrugation of the herringbone reconstruction underneath. This can explain the preservation of the herringbone reconstruction upon adsorption: It seems energetically more favorable to adjust adsorption position and conformation than to lift the herringbone reconstruction. Consequently, it is possible that the adsorption structures are commensurate with the reconstructed Au(111) surface.

The strong molecule/substrate interaction and the observed arching of the molecule also support the formation of the metal-ligand bond, which was observed for phase β. A threefold unit, where the N-atoms of three neighboring molecules point towards each other, would lead to an electrostatic repulsion between the molecules as the N-atoms are partially negatively charged. Such a motif is not possible in the gas phase. Consequently, the repulsion between the three N-atoms has to be screened by the surface. This can be done by the formation of a metal-ligand bond. There are two different possibilities for the formation of such a metal ligand bond: either by inclusion of ad-atoms into the molecular structure or by the slight displacement of a surface atom out of the surface. In general, the creation of metal ad-atoms on Au(111) surfaces leads to the lifting of the herringbone reconstruction.[12,42]

Additionally, elevated sample temperatures increase the number of ad-atoms considerably leading to an increased amount of metal-ligand bonds.[42] In our case, the herringbone reconstruction is not lifted, and annealing of the sample only leads to a slight increase of the amount of phase β. Thus, we propose that in the present case the metal-ligand bond is formed by the displacement of Au-atoms out of the surface due to the pulling of the partially negatively charged N-atoms of the cyano-group. So far, such a displacement of substrate atoms by cyano groups has been reported for tetracyanoquinodimethane (TCNQ) on Cu(100)[38] and for tetracyanoethylene (TCNE) on Ag(100).[39] The displacement of an Au-atom is less energy consuming than the creation of a free ad-atom, which would result in the lifting of the herringbone reconstruction. The strong CN/Au interaction expressed by the arching of the molecules, leads to the suggested displacement of the Au-atom. However, the displacement of the Au-atom closest to the N-atom could not be modeled with the DFT calculations as this would need three adjacent molecules pulling on the atom. It is assumed that the arching is not symmetric: The N-atom which forms the metal-ligand bond is probably closer to the surface than the N-atoms, which form the pores via dipolar antiparallel coupling, because this CN-CN bond is assumedly more stable when the CN-groups of neighboring molecules are parallel to each other.

4. Conclusions

In conclusion, we investigated the self-assembly of a bridged tricyano-substituted triarylamine derivative on Au(111). The two different adsorption structures phase α and phase β were analyzed in detail. The close-packed phase α is stabilized via dipolar coupling and hydrogen bonding while (the filled) phase β is stabilized by dipolar coupling, metal-ligand bonding (and hydrogen bonding). This means that all three known bonding motifs for cyano ligands were observed. Moreover and most remarkably, at least two cyano bonding motifs are needed for the formation of two of the three observed phases. This observation shows that for

our case a delicate interplay between molecular conformation, intermolecular interactions and molecule/substrate interactions leads to such a behavior. Importantly, the "active" role of the Au substrate needs to be considered which is responsible for both the correlation of the molecular orientation in dependence of the herringbone reconstruction and the arching of the molecules as shown by DFT calculations. This indicates that the role of the substrate needs to be taken into account when studying the self-assembly of functionalized molecules.

The strong molecule/substrate interactions results in the observed arching, which consequently leads to a large distance between the central N-atom and the Au substrate (4 Å). Hence, a weak interaction between this atom and the substrate is the case. It has been shown recently that a covalently bound two-dimensional porous sheet containing similar triarylamine derivatives is a ferromagnetic half-metal and as such it is potentially very interesting for spintronics.[43]

5. Experimental and Theoretical Details

5.1 Experimental Details

The experiments were performed in a two chamber ultra-high vacuum system with a base pressure < $5x10^{-10}$ mbar. The Au(111) single crystal was prepared by several cycles of Ar^+ sputtering and subsequent annealing at 350 °C. The molecules were sublimed in situ at a temperature of about 160 °C from a homebuilt evaporator while the sample was kept at room temperature during the molecule deposition. A quartz-crystal microbalance was used to monitor the deposition rate, which was kept constant at around 0.2 ML/min.

STM images were acquired at 77 K using a platinum-iridium tip in constant current mode. All bias voltages are with respect to the sample. The STM images were analyzed using the WSxM software,[44] while the correlation analysis was done using Python[45] and Qti-plot.[46] LEED patterns were recorded using an Omicron multichannel plate LEED. LEEDPAT was used to simulate the LEED patterns.[47]

5.2 Density functional Theory Calculations

All calculations were carried out within the framework of density functional theory (DFT), as embedded into the Vienna *ab-initio* Simulation Package (VASP)[48] version 5.2.12. The calculations were performed using the generalized gradient approximation (GGA) in the form of Perdew-Burke-Ernzerhof (PBE) as well as by including the non-local interactions through the self-consistent van der Waals density functional theory (optB88[35] and optB86b[49] functionals) as implemented in the VASP package.[47] The interaction between the valence electrons and ionic cores is described by the projector augmented wave (PAW) method.[50] A kinetic-energy cutoff of 400 eV was used for the wave functions. The molecules were introduced in a 25Åx35Åx10Å box for the dimers, and in a 35Åx35Åx10Å for the trimeric configuration. The k-points sampling used for the calculations was 1x1x1. We have performed an additional calculation using a 3x3x1 k-point sampling, and the change in the binding energy is found to be negligible, 8 meV for the trimetric case using the optB86b functional. The adsorption on the Au(111) surface was simulated by placing the molecule on one side of a (6x6) slab containing three layers of Au with 19 Å of vacuum separating the two surfaces. The k-point mesh of 3x3x1 is used for this calculation. During the structural relaxation, the atoms of the molecule as well as those of the first layer atoms of the substrate were allowed to relax. The bottom two layers of the substrate are kept fixed. The relaxation was done with a 0.01 eV/Å force criterion.

Supporting Information

Supporting Information is available online from the Wiley Online Library or from the author.

Acknowledgements

We thank Fei Song, Tuan Anh Pham and Luc Venema for their help during the experiments as well as for fruitful discussions. This work was supported by the Foundation for Fundamental Research on Matter (FOM), part of the Netherlands Organisation for Scientific Research (NWO), by the European Research Council (ERC-2012-StG 307760-SURFPRO), by NWO (Chemical Sciences, VIDI-grant No. 700.10.424 and VENI-grant No. 722.012.010) and by the Deutsche Forschungsgemeinschaft (DFG) as part of SFB953 (Project A5) "Synthetic Carbon Allotropes". AK acknowledges support from the U.S. Department of Energy Basic Energy Science under Contract No DE-FG02-11ER16243. The computational study used resources of the National Energy Research Scientific Computing Center, which is supported by the Office of Science of the U.S. Department of Energy under Contract No. DE-FG02-11ER16243.

Received: ((will be filled in by the editorial staff))

Revised: ((will be filled in by the editorial staff))

Published online: ((will be filled in by the editorial staff))

References

[1] a) G. Horowitz, *Adv. Mater.* **1998**, *10*, 365; b) Y. S. Zhao, H. Fu, A. Peng, Y. Ma, D. Xiao, J. Yao, *Adv. Mater.* **2008**, *20*, 2859; c) S. Fukuzumi, T. Kojima, *J. Mater. Chem.* **2008**, *18*, 1427.

[2] a) S. De Feyter, F. C. De Schryver, *Chem. Soc. Rev.* **2003**, *32*, 139; b) H. E. Hoster, M. Roos, A. Breitruck, C. Meier, K. Tonigold, T. Waldmann, U. Ziener, K. Landfester, R. J. Behm, *Langmuir* **2007**, *23*, 11570; c) A. Kühnle, *Curr. Opin. Colloid Interface Sci.* **2009**, *14*, 157; d) M. E. Cañas-Ventura, K. Aït-Mansour, P. Ruffieux, R. Rieger, K. Müllen, H. Brune, R. Fasel, *ACS Nano* **2011**, *5*, 457.

[3] a) J. V. Barth, J. Weckesser, C. Cai, P. Günter, L. Bürgi, O. Jeandupeux, K. Kern, *Angew. Chem. Int. Ed.* **2000**, *39*, 1230; b) J. A. Theobald, N. S. Oxtoby, M. A. Phillips, N. R. Champness, P. H. Beton, *Nature* **2003**, *424*,1029; c) R. Otero, M. Schöck, L. M. Molina, E. Lægsgaard, I. Stensgaard, B. Hammer, F. Besenbacher, *Angew. Chem. Int. Ed.* **2005**, *44*, 2270; d) A. Llanes-Pallas, M. Matena, T. Jung, M. Prato, M. Stöhr, D. Bonifazi, *Angew. Chem. Int. Ed.* **2008**, *47*, 7726.

[4] a) T. Yokoyama, S. Yokoyama, T. Kamikado, Y. Okuno, S. Mashiko, *Nature* **2001**, *413*, 619; b) N. Wintjes, J. Hornung, J. Lobo-Checa, T. Voigt, T. Samuely, C. Thilgen, M. Stöhr, F. Diederich, T. A. Jung, *Chem. Eur. J.* **2008**, *14*, 5794; c) M. Stöhr, S. Boz, M. Schär, M.-T. Nguyen, C. A. Pignedoli, D. Passerone, W. B. Schweizer, C. Thilgen, T. A. Jung, F. Diederich, *Angew. Chem. Int. Ed.* **2011**, *50*, 9982.

[5] a) N. Lin, A. Dmitriev, J. Weckesser, J. V. Barth, K. Kern, *Angew. Chem. Int. Ed.* **2002**, *41*, 4779; b) J. V. Barth, *Surf. Sci.* **2009**, *603*, 1533; c) C. S. Kley, J. Čechal, T. Kumagai, F. Schramm, M. Ruben, S. Stepanow, K. Kern, *J. Am. Chem. Soc.* **2012**, *134*, 6072.

[6] a) K. Tahara, S. Lei, J. Adisoejoso, S. De Feyter, Y. Tobe, *Chem. Commun.* **2010**, *46*, 8507; b) C. Arrigoni, G. Schull, D. Bléger, L. Douillard, C. Fiorini-Debuisschert, F. Mathevet, D. Kreher, A.-J. Attias, F. Charra, *J. Phys. Chem. Lett.* **2010**, *1*, 190; c) J.-H. Kim, K. Tahara, J. Jung, S. De Feyter, Y. Tobe, Y Kim, M. Kawai, *J. Phys. Chem. C* **2012**, *116*, 17082.

[7] L.-A. Fendt, M. Stöhr, N. Wintjes, M. Enache, T. A. Jung, F. Diederich, *Chem. Eur. J.* **2009**, *15*, 11139;

[8] D. Heim, K. Seufert, W. Auwärter, C. Aurisicchio, C. Fabbro, D. Bonifazi, J. V. Barth, *Nano Lett.* **2010**, *10*, 122.

[9] a) D. Heim, D. Écija, K. Seufert, W. Auwärter, C. Aurisicchio, C. Fabbro, D. Bonifazi, J. V. Barth, *J. Am. Chem. Soc.* **2010**, *132*, 6783; b) M. Koepf, F. Chérioux, J. A. Wytko, J. Weiss, *Coord. Chem. Rev.* **2012**, *256*, 2872.

[10] a) H. Liang, Y. He, Y. Ye, X. Xu, F. Cheng, W. Sun, X. Shao, Y. Wang, J. Li, K. Wu, *Coord. Chem. Rev.* **2009**, *253*, 2959; b) M. Matena, M. Stöhr, T. Riehm, J. Björk, S. Martens, M. S. Dyer, M. Persson, J. Lobo-Checa, K. Müller, M. Enache, H. Wadepohl, J. Zegenhagen, T. A. Jung, L. H. Gade, *Chem. Eur. J.* **2010**, *16*, 2079.

[11] P. A. Wood, S. J. Borwick, D. J. Watkin, W. D. S. Motherwell, F. H. Allen, *Acta Cryst. B* **2008**, *64*, 393.

[12] M. N. Faraggi, N. Jiang, N. Gonzalez-Lakunza, A. Langner, S. Stepanow, K. Kern, A. Arnau, *J. Phys. Chem. C* **2012**, *116*, 24558.

[13] G. Pawin, K. L. Wong, D. Kim, D. Sun, L. Bartels, S. Hong, T. S. Rahman, R. Carp, M. Marsella, *Angew. Chem. Int. Ed.* **2008**, *47*, 8442.

[14] a) S. Klyatskaya, F. Klappenberger, U. Schlickum, D. Kühnle, M. Marschall, J. Reichert, R. Decker, W. Krenner, G. Zoppellaro, H. Brune, J. V. Barth, M. Ruben, *Adv. Funct. Mater.* **2011**, *21*, 1230;

[15] D. Kühne, F. Klappenberger, R. Decker, U. Schlickum, H. Brune, S. Klyatskaya, M. Ruben, J. V. Barth, *J. Phys. Chem. C* **2009**, *113*, 17851.

[16] F. Klappenberger, D. Kühne, M. Marschall, S. Neppl, W. Krenner, A. Nefedov, T. Strunskus, K. Fink, C. Wöll, S. Klyatskaya, O. Fuhr, M. Ruben, J. V. Barth, *Adv. Funct. Mater.* **2011**, *21*, 1631.

[17] U. Schlickum, R. Decker, F. Klappenberger, G. Zoppellaro, S. Klyatskaya, M. Ruben, I. Silanes, A. Arnau, K. Kern, H. Brune, J. V. Barth, *Nano Lett.* **2007**, *7*, 3813.

[18] The synthesis and characterization of **1** will be published elsewhere.

[19] a) D. Hellwinkel, M. Melan, *Chem. Ber.* **1971**, *104*, 1001; b) D. Hellwinkel, M. Melan, *Chem. Ber.* **1974**, *107*, 616; c) D. Hellwinkel, W. Schmidt, *Chem. Ber.* **1980**, *113*, 358.

[20] a) J. E. Field, D. Venkataraman, *Chem. Mater.* **2002**, *14*, 962; b) Z. Fang, T.-L. Teo, L. Cai, Y.-H. Lai, A. Samoc, M. Samoc, *Org. Lett.* **2009**, *11*, 1; c) N. S. Makarov, S. Mukhopadhyay, K. Yesudas, J.-L. Brédas, J. W. Perry, A. Proń, M. Kivala, K. Müllen, *J.*

Phys. Chem. A **2012**, *116*, 3781; d) F. Schlütter, F. Rossel, M. Kivala, V. Enkelmann, J.-P. Gisselbrecht, P. Ruffieux, R. Fasel, K. Müllen, *J. Am. Chem. Soc.* **2013**, *135*, 4550.

[21] a) C. Liu, Y. Li, Y. Zhang, C. Yang, H. Wu, J. Qin, Y. Cao, *Chem. Eur. J.* **2012**, *18*, 6928; b) Z. Fang, V. Chellappan, R. D. Webster, L. Ke, T. Zhang, B. Liu, Y.-H. Lai, *J. Mater. Chem.* **2012**, *22*, 15397; c) K. Schmoltner, F. Schlütter, M. Kivala, M. Baumgarten, S. Winkler, R. Trattnig, N. Koch, A. Klug, E. J. W. List, K. Müllen, *Polym. Chem.* **2013**, DOI: 10.1039/c3py00089c.

[22] a) D. Kim, C. Kim, H. Choi, K. Song, M.-S. Kang, J. Ko, *J. Photochem. Photobiol. A: Chem.* **2011**, *219*, 122; b) K. Do, D. Kim, N. Cho, S. Paek, K. Song, J. Ko, *Org. Lett.* **2012**, *14*, 222.

[23] a) M . Böhringer, W.-D. Schneider, *Surf. Rev. Lett.* **2000**, 7, 661; b) I. Fernandez-Torrente, S. Monturet, K. J. Franke, J. Fraxedas, N. Lorente, J. I. Pascual, *Phys. Rev. Lett.* **2007**, 99, 176103; c) L. Gao, Q. Liu, Y. Y. Zhang, N. Jiang, H. G. Zhang, Z. H. Cheng, W. F. Qui, S. X. Du, Y. Q. Liu, W. A. Hofer, H.-J. Gao, *Phys. Rev. Lett.* **2008**, 101, 197209; d) J. Henzl, K. Morgenstern, *Phys. Chem. Chem. Phys* **2010**, 12, 6035.

[24] J. Reichert, M. Marschall, K. Seufert, D. Ecija, W. Auwärter, E. Arras, S. Klyatskaya, M. Ruben, J. V. Barth, *J. Phys. Chem. C* **2013**, 117, 12858.

[25] M. Bieri, S. Blankenburg, M. Kivala, C. A. Pignedoli, P. Ruffieux, K. Müllen, R. Fasel, *Chem. Commun.* **2011**, *47*, 10239.

[26] J. V. Barth, H. Brune, G. Ertl, R. J. Behm, *Phys. Rev. B* **1990**, *42*, 9307.

[27] a) S. M. Barlow, R. Raval, *Surf. Sci. Rep.* **2003**, *50*, 201; b) K.-H. Ernst, *Phys. Status Solidi B* **2012**, *249*, 2057.

[28] Y. Okuno, T. Yokoyama, S. Yokoyama, T. Kamikado, S. Mashiko, *J. Am. Chem. Soc.* **2002**, *124*, 7218.

[29] The correlation function expresses the probability that after a certain number of molecules (N) a molecule has the same orientation as the starting molecule. A probability

larger than 0.5 at position N means that after N molecules there is a higher probability to find a molecule pointing in the same direction as the molecule at the starting position. On the contrary, a probability less than 0.5 indicates anti-correlation and thus, the preference that the molecule is rotated after N positions with respect to the starting molecule.

[30] E. Arras, A. P. Seitsonen, F. Klappenberger, J. V. Barth, *Phys. Chem. Chem. Phys.*, **2012**, *14*, 15995.

[31] S. Kitagawa, R. Kitaura, S.-i. Noro*, Angew. Chem. Int. Ed.* **2004**, *43*, 2334.

[32] a) S. Stepanow, N. Lin, D. Payer, U. Schlickum, F. Klappenberger, G. Zoppellaro, M. Ruben, H. Brune, J. V. Barth, K. Kern, *Angew. Chem. Int. Ed.* **2007**, *46*, 710; b) L. Bartels, *Nature Chem.* **2010**, *2*, 87.

[33] B. Cui, H.-J. Yan, D. Wang, L.-J. Wan, *J. Electroanalytical Chem.* **2013**, *688*, 237.

[34] J. Björk, M. Matena, M. S. Dyer, M. Enache, J. Lobo-Checa, L. H. Gade, T. A. Jung, M Stöhr, M. Persson, *Phys. Chem. Chem. Phys.* **2010**, 12, 8815.

[35] J. Klimeš, D. R. Bowler, A. Michaelides, *J. Phys. Condens. Matter* **2010**, *22,* 022201.

[36] H. Yildirim, A. Kara, *J. Phys. Chem. C* **2013**, *117*, 2893.

[37] a) M. Dion, H. Rydberg, E. Schroder, D. C. Langreth, B. I. Lundqvist, *Phys. Rev. Lett.* **2004**, *92,* 246401; b) J. Carrasco, B. Santra, J. Klimeš, A. Michaelides, *Phys. Rev. Lett.* **2011**, *106,* 026101.

[38] T.-C. Tseng, C. Urban, Y. Wang, R. Otero, S. L. Tait, M. Alcamí, D. Écija, M. Trelka, J. M. Gallego, N. Lin, M. Konuma, U. Starke, A. Nefedov, A. Langner, C. Wöll, M. Ángeles Herranz, F. Martín, N. Martín, K. Kern, R. Miranda, *Nature Chem.* **2010**, *2*, 374.

[39] D. Wegner, R. Yamachika, X. Zhang, Y. Wang, M. F. Crommie, N. Lorente, *Nano Lett.* **2013**, *13*, 2346.

[40] a) A. Ferretti, C. Baldacchini, A. Calzolari, R. D. Felice, A. Ruini, E. Molinari, M. Betti, *Phys. Rev. Lett.* **2007**, *99*, 046802; b) K. Müller, A. P. Seitsonen, T. Brugger, J. Westover, T. Greber, T. Jung, A. Kara, *J. Phys. Chem. C* **2012**, *116*, 23465.

[41] I. Fernández Torrente, K. J. Franke, J. I. Pascual, *Int. J. Mass Spectr.* **2008**, *277*, 269.

[42] Z. Shi, N. Lin, *J. Am. Chem. Soc.* **2009**, *131*, 5376.

[43] E. Kan, W. Hu, C. Xiao, R. Lu, K. Deng, J. Yang, H. Su, *J. Am. Chem. Soc.* **2012**, *134*, 5718.

[44] I. Horcas, R. Fernández, J. M. Gómez-Rodríguez, J. Colchero, J. Gómez-Herrero, A. M. Baro, *Rev. Sci. Instr.* **2007**, *78*, 013705.

[45] http://www.python.org/

[46] http://soft.proindependent.com/qtiplot.html

[47] http://www.fhi-berlin.mpg.de/KHsoftware/LEEDpat/

[48] G. Kresse, J. Furthmüller, *Phys. Rev. B.* **1996**, *54*, 11169.

[49] J. Klimeš, D. R. Bowler, A. Michaelides, *Phys. Rev. B,* **2011,** *83,* 19513.

[50] a) P. Blöchl, *Phys. Rev. B* **1994**, *50*, 17953; b) G. Kresse, D. Joubert, *Phys. Rev. B* **1999**, *59*, 1758.

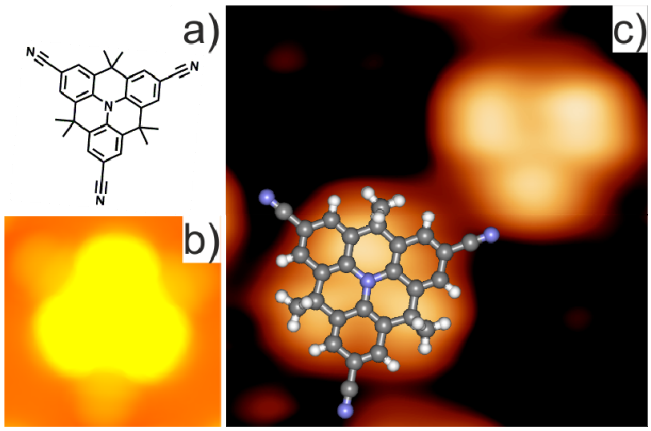

Figure 1. a) Chemical structure of **1**; b) simulated STM image of **1**; c) high-resolution STM image for two molecules. The molecular structure is superimposed for the lower left molecule (2x2 nm^2, U = 3.0 V, I = 70 pA).

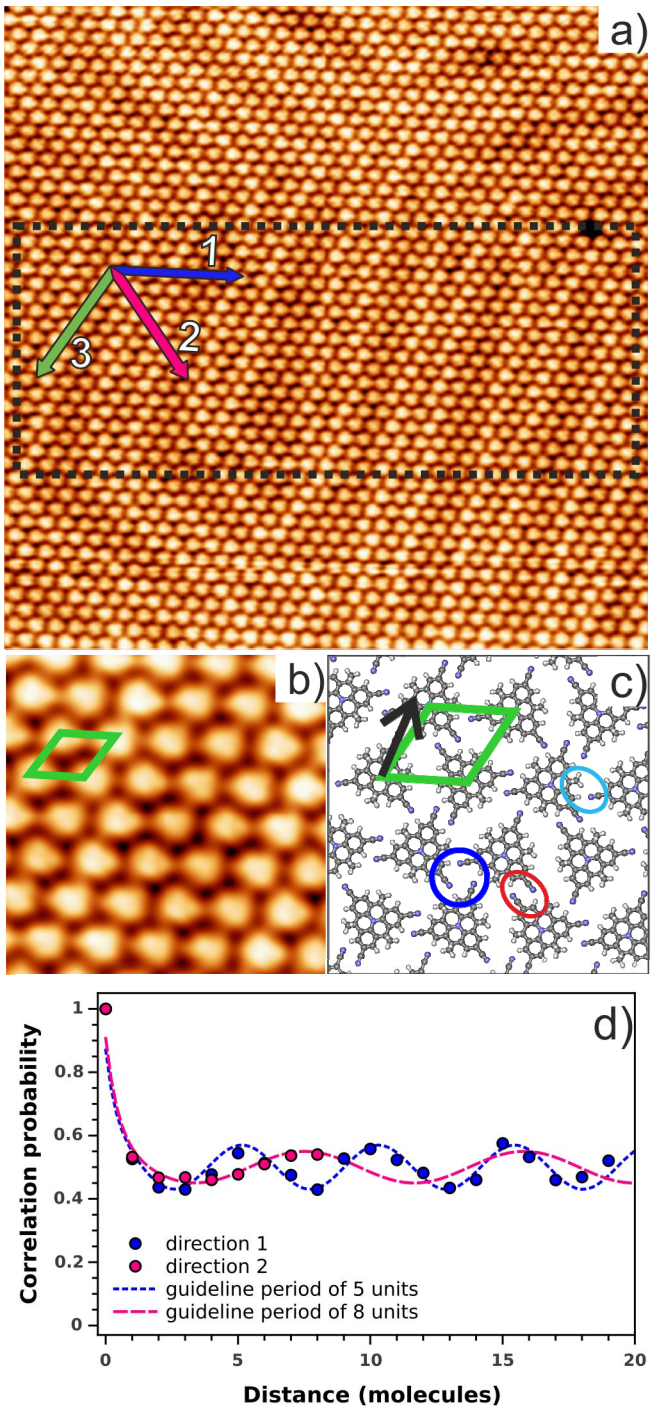

Figure 2. Close-packed phase α: a) Overview STM image (40x40 nm^2, U = 1.8 V, I = 70 pA) with the herringbone reconstruction of the Au(111) surface visible through the molecular layer. b) High-resolution STM image (7x7 nm^2, U = 1.2 V, I = 40 pA) with the unit cell marked in green. c) Tentative model of the molecular arrangement, with the unit cell marked in green, while the black arrow indicates the [$1\bar{1}0$]-direction of the Au(111) surface. The differently colored ovals indicate the different bonding motifs. d) Correlation of the molecular

orientation along direction 1 (blue) and along direction 2 (pink); the black rectangle in a) indicates the area which was used to calculate the correlation.

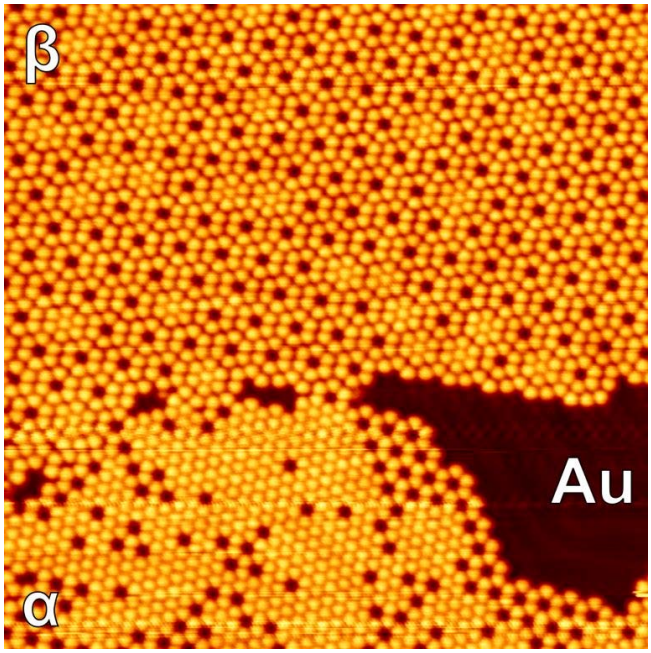

Figure 3. STM image (50x50 nm^2, U = 1.4 V, I = 40 pA) for a coverage of 0.65 ML of **1**. Two different molecular arrangements are visible: in the lower part the molecules are arranged in the close-packed phase α which exhibits various vacancies, while in the upper part phase β is formed.

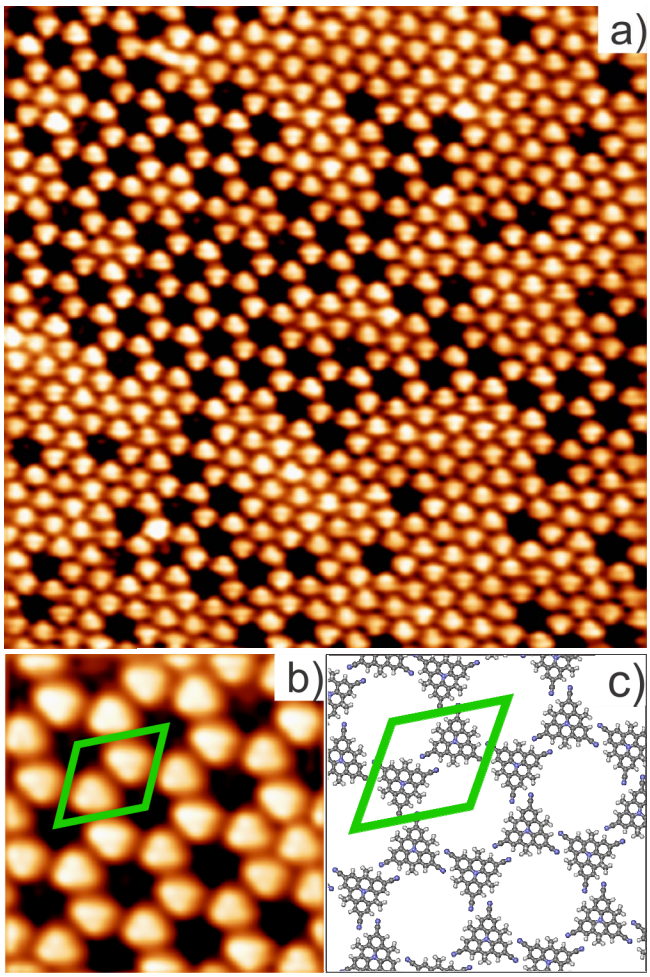

Figure 4. Porous phase *α*: a) Overview STM image (25x25 nm^2, U = 2.0 V, I = 70 pA) showing the coexistence of porous and close-packed areas. b) High-resolution STM image of the porous phase *α* (7x7 nm^2, U = 2.0 V, I = 70 pA), with the unit cell marked in green. c) Tentative model of the molecular arrangement with the unit cell marked in green.

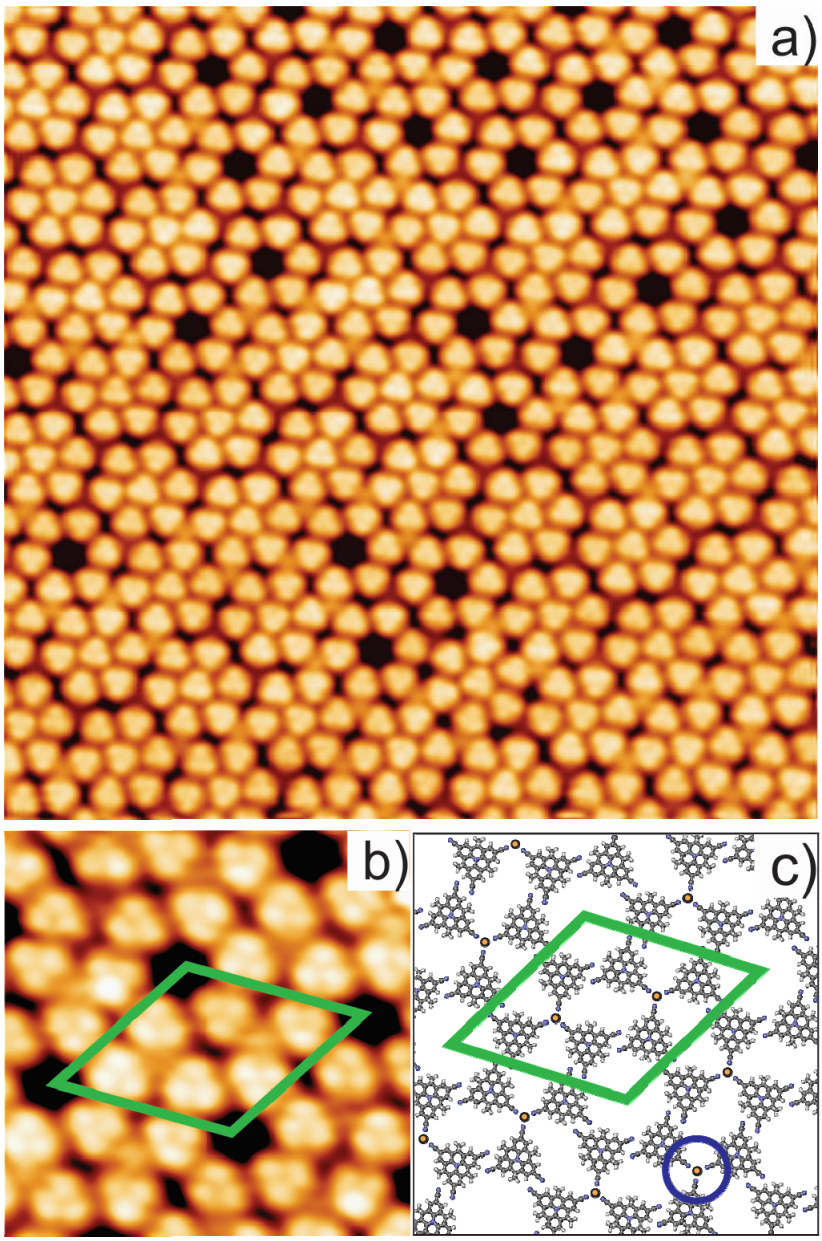

Figure 5. Phase β: a) Overview STM image (25x25 nm^2, U = 2.0 V, I = 30 pA). b) High-resolution STM image (7x7 nm^2, U = 3.0 V, I = 140 pA), with the unit cell marked in green. Increased contrast is observed at the places where three pores meet. This is attributed to a metal-ligand bonding between three CN-groups and one Au atom. c) Tentative model of the molecular arrangement with the unit cell marked in green. The Au-atoms, which are involved in metal-ligand bonding, are drawn in yellow.

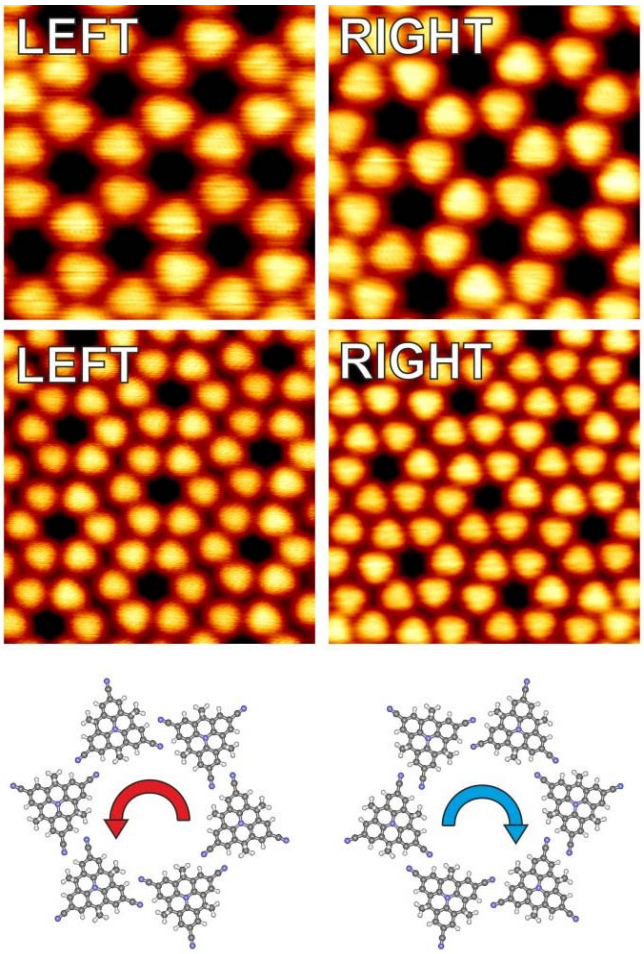

Figure 6. Organizational chirality for the porous phase α (top row) and phase β, (center row). The bottom row shows the molecular model for an individual pore. Left panel: left handed chirality, right panel: right handed chirality. Top: porous phase α, 8x8 nm^2 (left: U = 1.2 V, I = 30 pA, right: U = 1.2 V, I = 20 pA), center: phase β, 12x12 nm^2 (left: U = 1.2 V, I = 30 pA, right: U = –1.2 V, I = 30 pA).

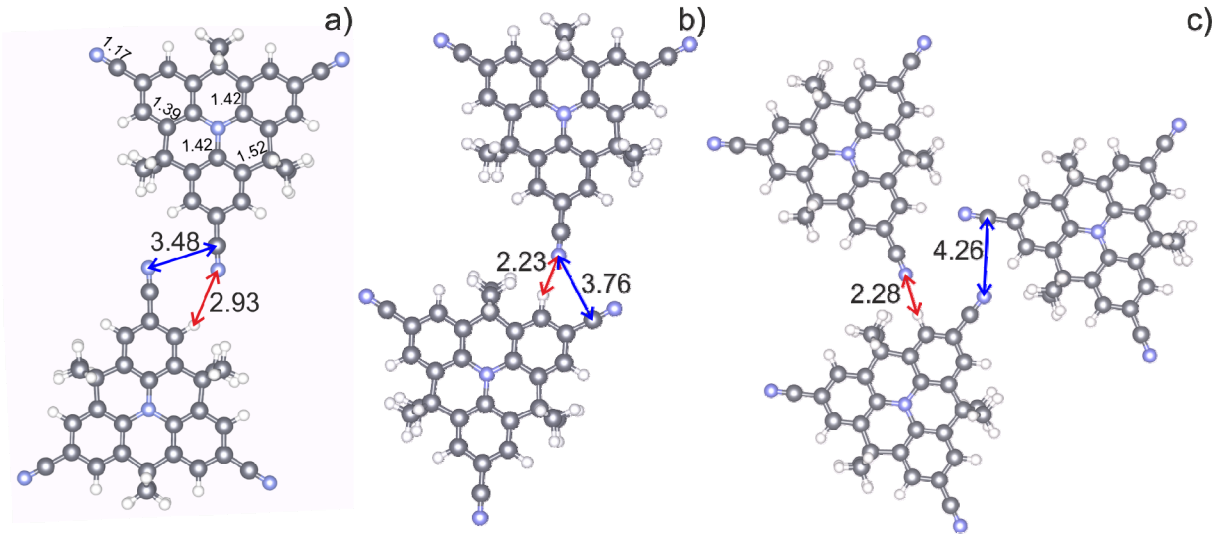

Figure 7. Optimized gas phase bonding motifs calculated with OptB86b and the bond lengths for a single molecule for a) CN-CN, b) CN-HC and c) trimeric unit motifs. The bond distances, which are marked with red and blue arrows as well as intramolecular bond lengths are given in Å.

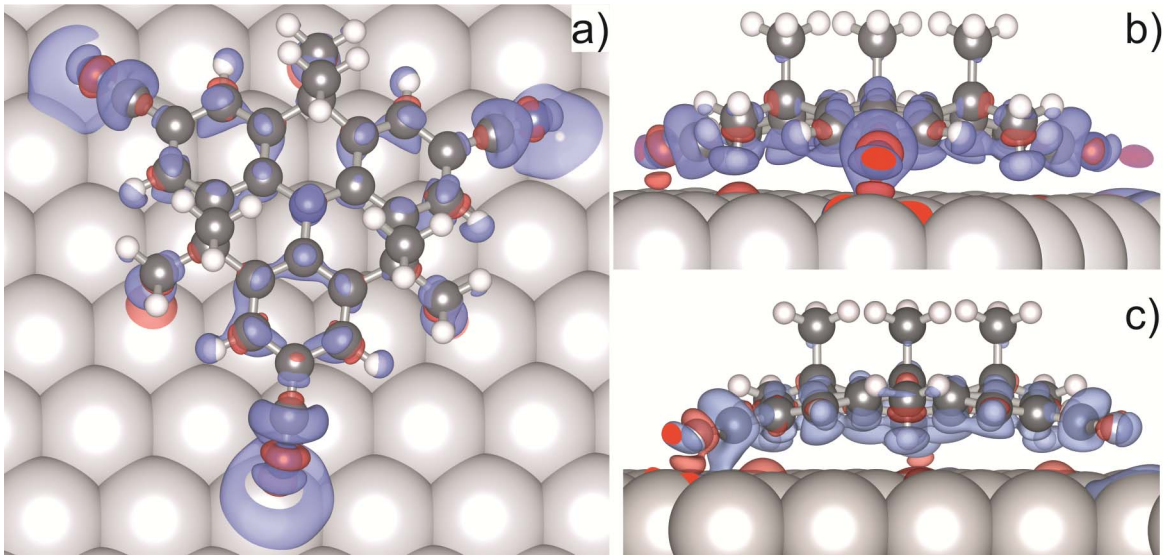

Figure 8. Adsorption structure of **1** on Au(111) and charge density difference (Iso-surface=0.6x10^{-3} eÅ^{-3}) obtained with optB86b; blue represents depletion and red accumulation of charge. a) Top view, b) side view, viewed from a CN-group and c) side view, viewed from a methyl group.

Table 1. Bond lengths* (in Å) for the studied bonding motifs in the gas phase and binding energies per molecule-molecule bond (in meV).

Motifs	$\mathbf{d_{C\text{-}N}}$	$\mathbf{d_{N\text{-}H}}$	$\mathbf{d_{mol\text{-}mol}}$	$\mathbf{E_{bind}}$
CN-CN	3.51	2.99	14.08	188
	3.48	2.93	14.01	312
	3.47	2.85	13.93	328
	3.3 [a]	2.2 [a]	13.2 [a]	
CN-HC	3.75	2.23	12.96	104
	3.76	2.23	12.95	228
	3.76	2.18	12.93	212
	3.7 [a]	1.8 [a]	13.2 [a]	
trimeric	4.06	2.29	13.24	165
	4.26	2.28	13.23	273
	4.04	2.29	13.23	272
	3.5 [a]	1.9 [a]	13.2 [a]	

* The first, second and third values in each column are the results of PBE, optB86b, and optB88 functionals, respectively. [a] values measured from the tentative structure models shown in Figure 2c.

The table of contents entry

The self-assembly of planarized cyano-substituted triarylamines on Au(111) is studied with STM and DFT calculations. A complex interplay of intermolecular and molecule/substrate interactions leads to the formation of different phases, stabilized by a combination of dipolar coupling, hydrogen bonding, and metal-ligand interactions.

Keyword (see list) self-assembly, dipolar coupling, cyano functional group, scanning tunneling microscopy, triarylamines

*Stefano Gottardi [†], Kathrin Müller [†], *, Juan Carlos Moreno-López, Handan Yildirim, Ute Meinhardt, Milan Kivala*, Abdelkader Kara, Meike Stöhr**

([†]contributed equally)

Title

Cyano-Functionalized Triarylamines on Au(111): Competing Intermolecular vs. Molecule/Substrate Interactions

ToC figure ((Please choose one size: 55 mm broad × 50 mm high **or** 110 mm broad × 20 mm high. Please do not use any other dimensions))